2013 European Control Conference (ECC)
July 17-19, 2013, Zürich, Switzerland.

Control of Airborne Wind Energy Systems Based on Nonlinear Model Predictive Control & Moving Horizon Estimation

Sébastien Gros, Mario Zanon and Moritz Diehl

Abstract— **Among the several problems arising in the Airborne Wind Energy paradigm, an essential one is the control of the tethered airfoil trajectory during power generation. Tethered flight is a fast, strongly nonlinear, unstable and constrained process, motivating control approaches based on fast Non-linear Model Predictive Control. In this paper, a computationally efficient model is proposed, based on Differential-Algebraic equations. A control scheme based on Nonlinear Model Predictive Control (NMPC) and an estimator based on Moving Horizon Estimation (MHE) is proposed to handle the wind turbulences. In order to make a real-time application of Non-linear Model Predictive Control possible, a Real-Time Iteration scheme is proposed.**

Keywords **: flight control, fast NMPC & MHE, trajectory tracking, Real-time iteration, Optimal Control**

I. INTRODUCTION

To overcome the major difficulties posed by the exponentially growing size and mass of conventional wind turbine generators [17], [3], the Airborne Wind Energy (AWE) paradigm shift proposes to get rid of the structural elements not directly involved in power generation. The research directions theoretically demonstrated as the most efficient and consensually recognized as the most promising propose to perform power generation through crosswind flight [18], which essentially consists in extracting power from the airflow by flying an airfoil tethered to the ground at a high velocity across the wind direction. Power can be generated by a) performing a cyclical variation of the tether length, together with cyclical variation of the tether tension or b) by using on-board turbine(s), transmitting the power to the ground via the tether. In this paper, the first option is considered.

Because it involves a much lighter structure, a major advantage of power generation based on crosswind flight over conventional wind turbines is that higher altitude can be reached and a larger swept area can arguably be achieved, hence reaching wind resources that cannot be tapped into by conventional wind turbines.

While the potential efficiency of the principle is established in theory, a major research effort is still required to address the several engineering difficulties posed by its implementation and achieve the efficiency required for its industrial development. Among the several issues that have been identified so far, the control of tethered flight is a major challenge. The control problems currently recognized as most crucial are a) control during power generation b) control during airfoils retrieval and c) control during airfoils launch. This paper addresses the problem of control during power generation.

In [10], a reliable methodology for designing power-generating periodic trajectories is presented. Because the actuators limitations and process constraints are significantly activated by the resulting orbits and because the process dynamics are strongly nonlinear, this paper proposes to tackle tethered flight control through Nonlinear Model Predictive Control (NMPC).

Classical NMPC approaches suffer from two major drawbacks when applied to fast processes: a) the computational time required to compute input updates can be prohibitively large in a real-time scenario, and b) the latency between the computation of the process state estimation and the corresponding process inputs update can be large, hence imposing a significant delay between measurement and the resulting control actions.

Because tethered flight is a fast, unstable and perturbed system, both issues are critical for the applicability of the NMPC scheme to a real power-generating airfoil system. To address these issues, the Real-Time Iteration (RTI) scheme has been proposed in [5], [16]. RTI proposes to reduce the computational time required by conventional NMPC scheme by performing a single, full Newton-type iteration per control input update instead of several SQP steps. Moreover, the RTI scheme proposes to reduce the control update latency by preparing most of the computations without a priori knowledge of the process state so as to perform the input update in a negligible time when the process state estimation becomes available.

In [12], a fast NMPC scheme for the control of a 6-DOF kite model in wind turbulences was proposed and tested in simulation. It was assumed in that paper that the pitch-roll-yaw acceleration rates are directly controlled, by e.g. fast inner loops. In contrast, this paper proposes to handle directly in the NMPC scheme the aerodynamic interaction of the kite with the airmass. A scheme combining NMPC and MHE for the tracking of power-generating trajectories is presented, resulting in computational performances that are suitable for a real-time application. So as to propose a more realistic scenario, the case study presented in the simulations considers a Von Karman [19] turbulent wind model as the process disturbance.

This paper is organized as follows. The process model is presented in Section II, the control scheme is proposed in Section III. Simulation results are presented in Section IV.

S. Gros, M. Zanon and M. Diehl are with the Optimization in Engineering Center (OPTEC), K.U. Leuven, Kasteelpark Arenberg 10, B-3001 Leuven-Heverlee, Belgium. sgros@esat.kuleuven.be

Conclusions are proposed in Section V.

Contribution of the paper: this paper proposes a control scheme based on fast MHE and NMPC for the control of a 6-DOF model for tethered flight. The control scheme is tested in simulations using elaborate sensor information and in the presence of a turbulent wind field.

II. Model of the system

The model used in this paper is described in detail in [10], it is briefly recalled here. The wing is considered as a rigid body having 6 degrees of freedom (DOF). An orthonormal right-hand reference frame E is chosen s.t. a) the wind is blowing in the E_1-direction, b) the vector E_3 is opposed to the gravitational acceleration vector g. The origin of the coordinate system coincides with the generator. The position of the wing center of mass in the reference frame E is given by the coordinate vector $p = [x,y,z]^T$. The tether is approximated as a rigid link of (time-varying) length r that constrains p to evolve on the 2-dimensional manifold $C = \frac{1}{2}\left(p^T p - r^2\right) = 0$. Such an assumption requires that the tether is always under tension. In this paper, it is assumed that the second time derivative of the tether length, i.e. $\ddot{r} \in \mathbb{R}$ is a control variable.

A right-hand orthonormal reference frame e is attached to the wing s.t. a) the basis vector e_1 spans the wing longitudinal axis, pointing in the forward direction and is aligned with the wing chord, b) the basis vector e_3 spans the vertical axis, pointing in the upward direction. The origin of e is attached to the center of mass of the wing. In the following, the vectors $e_{1,2,3}$ are given in E. The description of the wing attitude is given by the rotation matrix R:

$$R = \left[\begin{array}{ccc} e_1 & e_2 & e_3 \end{array}\right],$$

Because the set of coordinates $\{x,y,z\}$ describes the position of the center of mass of the wing, the translational dynamics and the rotational dynamics are separable, and the wing rotational dynamics reduce to:

$$\dot{R} = R\omega_\times, \quad J\dot{\omega} + \omega \times J\omega = T, \tag{1}$$

$$\langle e_i, e_j \rangle_{t=t_c} = \delta_{ij}, \tag{2}$$

where $\omega_\times \in SO(3)$ is the skew matrix yielded by the angular velocity vector ω, and $T \in \mathbb{R}^3$ is the moment vector in e. Because $\langle e_i, \dot{e}_j \rangle = 0$, the orthonormality conditions $\langle e_i, e_j \rangle_{t=t_c} = \delta_{ij}$ enforced at any arbitrary time t_c are preserved by the dynamics (1). Yet, for long integration times, a correction of the numerical drift of the orthonormality of R may be needed (see e.g [11] for a stabilization of the orthonormality of R).

Using Lagrange mechanics, and after index-reduction, the equations of motion of the system are in the index-1 DAE form:

$$\left[\begin{array}{cc} m\cdot I_3 & p \\ p^T & 0 \end{array}\right]\left[\begin{array}{c} \ddot{p} \\ \lambda \end{array}\right] = \left[\begin{array}{c} F - \mathcal{V}_p - \dot{m}\dot{p} \\ \dot{r}^2 + r\ddot{r} - \dot{p}^T\dot{p} \end{array}\right], \tag{3}$$

$$C(t=0) = \frac{1}{2}\left(p^T p - r^2\right)_{t=t_c} = 0, \tag{4}$$

$$\dot{C}(t=0) = \left(p^T\dot{p} - r\dot{r}\right)_{t=t_c} = 0,$$

where I_3 is the 3×3 identity matrix and F the sum of the forces applied at the center of mass of the wing. The force in the tether and the mechanical power extracted from the wing are readily given by:

$$F_T = \|\lambda p\| = \lambda r, \qquad \dot{E} = F_T\dot{r} = \lambda r\dot{r} \tag{5}$$

Introducing the relative velocity v, i.e. the velocity of the wing w.r.t the air mass given in the reference frame E by:

$$v = \left[\begin{array}{ccc} \dot{x} & \dot{y} & \dot{z} \end{array}\right]^T - W^T, \tag{6}$$

where $W \in \mathbb{R}^3$ is the local wind velocity field (see II-A). The lift and drag forces, F_L and F_D acting on the wing are therefore given by:

$$F_L = \frac{1}{2}\rho A C_L \|v\|\,(v \times e_2), \qquad F_D = -\frac{1}{2}\rho A C_D \|v\| v. \tag{7}$$

In this model, it is assumed that the lift and drag coefficients C_L and C_D depend on the angle of attack α and side-slip angle β only. For some range $\alpha_{\min} \le \alpha \le \alpha_{\max}$ and $-\beta_{\max} \le \beta \le \beta_{\max}$, C_L and C_D are well approximated by [20], [4]:

$$\begin{aligned} C_L &= C_L^0 + C_L^\alpha \alpha, \\ C_D &= C_D^0 + C_D^\alpha \alpha^2 + C_D^\beta \beta^2, \end{aligned}$$

Defining $\nu = [\nu_1, \nu_2, \nu_3]^T$ as the coordinate vector of the relative velocity v projected in the wing frame e, i.e.:

$$\nu = R^T v,$$

for small angles α and β can be approximated by [20]:

$$\alpha = -\frac{\nu_3}{\nu_1}, \qquad \beta = \frac{\nu_2}{\nu_1}.$$

In this paper, the approximate tether drag model proposed in [14] is used. The tether drag is lumped into a single equivalent force F_T^D (projected in frame e) acting at the wing center of mass (see [14]) given by:

$$F_T^D = -\frac{1}{8}\rho D_T C_T r \|[v]_e - \dot{r}e_r\|\,([v]_e - \dot{r}e_r),$$

where $e_r = r^{-1}\left[\begin{array}{ccc} x & y & z \end{array}\right]^T$, D_T is the tether diameter, and C_T the tether drag coefficient. The sum of the forces F in (3) acting at the wing center of mass is given by $F = F_A + F_T^D$.

The vector of aerodynamic moment T_A is given by:

$$T_A = \frac{1}{2}\rho A \|v\|^2 \left[\begin{array}{c} C_R \\ C_P \\ C_Y \end{array}\right], \tag{8}$$

where

$$\begin{aligned} C_R &= -D_R\left(\omega_1 - e_1^T\Omega\right) - A_R\left(\omega_3 - e_3^T\Omega\right) + C_R^a u_a \\ C_P &= C_P\alpha + C_P^T\alpha_T + C_P^e u_e \\ C_Y &= A_Y\left(\omega_1 - e_1^T\Omega\right) + C_Y^T\beta_T + C_Y^r u_r, \end{aligned} \tag{9}$$

and $\Omega \in \mathbb{R}^3$ is the local angular velocity vector of the airmass yielded by the turbulences, given in frame e (see Section II-A), so that $e_i^T\Omega$ is the i^{th} component of the angular velocity of the airmass turbulences given in the wing reference frame

TABLE I

WIND PARAMETERS

Parameter	Value
W_0	10 [m/s]
z_0	100 [m]
z_0	0.1 [m]
Wind velocity at 6 [m]	2 [m/s]
High-altitude turbulence	10^{-3} [-] (moderate)
Scale length at med/high altitude	533 [m]
Wing span	30 [m]

E. Angles α_{T}, β_{T} are the tail angle of attack and side-slip angle, given by:

$$\alpha_{\mathrm{T}} = -\frac{v_3 + L_{\mathrm{T}}\left(\omega_2 - e_2^T \Omega\right)}{v_1}, \qquad \beta_{\mathrm{T}} = \frac{v_2 - L_{\mathrm{T}}\left(\omega_3 - e_3^T \Omega\right)}{v_1}$$

where L_{T} is the tail effective length.

In the following, $\mathcal{U} = [\ddot{r}, \dot{u}_{\mathrm{a}}, \dot{u}_{\mathrm{e}}, \dot{u}_{\mathrm{r}}]^T \in \mathbb{R}^4$ are the system control input, and $\mathcal{X} = \left[x, y, z, \dot{x}, \dot{y}, \dot{z}, e_1^T, e_2^T, e_3^T, \omega_1, \omega_2, \omega_3, r, \dot{r}, u_{\mathrm{a}}, u_{\mathrm{e}}, u_{\mathrm{r}}\right]^T \in \mathbb{R}^{23}$ are the system state trajectories.

A. Wind model

It is assumed here that the wind is the superposition of a laminar, logarithmic wind shear model blowing in the uniform x-direction with a Von Karman [19] turbulence model. The vector fields $W(z,t)$ and $\Omega(z,t)$ in (6) and (9) are given by :

$$W(z,t) = \begin{bmatrix} W_0 \frac{\log(z/z_{\mathrm{r}})}{\log(z_0/z_{\mathrm{r}})} + \Gamma_1(t) & \Gamma_2(t) & \Gamma_3(t) \end{bmatrix} \qquad (10)$$
$$\Omega(t) = \begin{bmatrix} \Omega_1(t) & \Omega_2(t) & \Omega_3(t) \end{bmatrix}$$

where $W_0 \in \mathbb{R}$ is the wind velocity at altitude z_0 and z_r is the ground roughness. The wind and Von Karman parameters are displayed in table I. The resulting 10 min wind profiles used in the proposed simulations are displayed in Fig. 5. Since is assumes a level flight at constant velocity, the Von Karman model is not the most appropriate turbulence model for AWE systems, and should not be used for certification purposes. However, it is arguably a simple mean to test control algorithms. Better turbulence models that could be used for e.g. load assessment are the object of current research.

III. CONTROL SCHEME

This paper presents a control scheme based on MHE & NMPC for the proposed AWE system. In this section, the formulation and implementation of the MHE and NMPC scheme is presented.

A. Multiple-shooting

Because the model dynamics are unstable and because estimation and prediction horizons T_{E} and T_{P} of several seconds need to be considered in the MHE and NMPC schemes, the underlying optimal control problems (OCPs) shall be tackled using simultaneous approaches [1]. A direct multiple-shooting discretization of the dynamics was chosen [2], where the model states and inputs are discretized on a uniform time grid $t_{i-N_{\mathrm{E}}}, ..., t_i, ..., t_{i+N_{\mathrm{P}}}$ around the current time t_i via numerical integration over the time intervals $[t_k, t_{k+1}]$. The vector of control input $\mathcal{U}$ is discretized as piecewise constant over the shooting intervals such that $\mathcal{U}(t \in [t_k, t_{k+1}[) = \mathcal{U}_k$, and the state vector $\mathcal{X}(t)$ discretized as $\mathcal{X}(t_k) = \mathcal{X}_k$. Because the integration of the shooting intervals is carried out using an integrator with error control, the resulting discrete dynamic system represents accurately the continuous system. The inequality constraints are discretized on the same time grid. The discretized OCPs are medium-scale structured Non-Linear Programs (NLP).

B. MHE formulation

The model proposed in Section II is subject to the wind $W(z,t)$ with the unknown translational turbulences Γ and rotational turbulences Ω. It was observed in simulations that assuming a laminar wind flow in the MHE scheme yields inaccurate state estimations and eventually results in the failure of the MHE+NMPC scheme. Taking into account at least the translational turbulences is crucial for the robustness of the control scheme to wind turbulences.

Wind turbulences can be modeled as elaborate stochastic processes, which have been extensively studied in the literature. However, making strong assumptions on the statistical properties of the wind turbulences for the control of AWE system can yield to poor control performances when such assumptions are not correct. In the proposed MHE formulation, it assumed that $\dot{\Gamma}(t)$ and $\dot{\Omega}(t)$ are Gaussian white noise, and introduced as fictitious control variables in the MHE formulation. Moreover, because of actuator noise and inaccuracy, the control policies computed by the NMPC scheme may not be perfectly implemented on the system, therefore the system inputs are also decision variables in the MHE scheme, and their deviation from the inputs provided by the NMPC penalized by the weight R_{E}.

Following the argument developed in [13], the consistency conditions (2) and (4) are enforced in the MHE scheme at the current time t_i, i.e. t_c was chosen as $t_{\mathrm{c}} = t_i$. Defining the set of decision variables $w_{\mathrm{E}} = \left[\mathcal{X}\ \mathcal{U}\ \dot{W}\ \dot{\Omega}\right]$, at the current time t_i the MHE scheme reads:

$$\left\{\hat{\mathcal{X}}_i, \hat{\mathcal{U}}, \hat{\Gamma}_i, \hat{\Omega}_i\right\} = \arg\min_{w_{\mathrm{E}}} \sum_{k=i}^{i-N_{\mathrm{E}}} \|\bar{Y}_k - Y(\mathcal{X}_k)\|^2_{Q_{\mathrm{E}}} + \|\bar{\mathcal{U}}_k - \mathcal{U}_k\|^2_{R_{\mathrm{E}}} + \|\dot{\Gamma}_k\|^2_{T_{\mathrm{T}}} + \|\dot{\Omega}_k\|^2_{T_{\mathrm{R}}} \qquad (11)$$
$$\text{s.t.} \quad (1) - (10)$$

where $\bar{Y}_k$ is the set of measurements available at time t_k, and $Y(\mathcal{X}_k)$ the corresponding set of measurement obtained from the state of the model $\mathcal{X}_k$.

1) Available sensors & measurement noise: In this paper, it is proposed to perform the estimation based on sensors that are commonly available to AWE systems and airborne applications. Data from IMU and GPS can already provide a reasonably good estimation of the wing attitude [9], however, the availability and fusion of more sensor data helps reducing the covariance of the state estimation. The list of

TABLE II
AVAILABLE SENSORS FOR MHE

Sensor	Measurement	σ
IMU	Linear accelerations in frame e	$5\,\mathrm{cm}\cdot\mathrm{s}^{-2}$
IMU	Angular velocities ω	$1\,\mathrm{deg}\cdot\mathrm{s}^{-1}$
GPS	Absolute positions p	$0.1\,\mathrm{m}$
GPS	Absolute velocities $\dot{p}$	$0.6\,\mathrm{m}\cdot\mathrm{s}^{-1}$
Variometer	Absolute vertical velocity $\dot{z}$	$0.5\,\mathrm{m}\cdot\mathrm{s}^{-1}$
Tether encoder	Tether length & velocity r,$\dot{r}$	$5\,\mathrm{m}$, $1\,\mathrm{m}\cdot\mathrm{s}^{-1}$
Tether gauge	Tether tension F_T	$500\,\mathrm{N}$
Pitot tube	Long. relative velocity v_l	$1\,\mathrm{m}\cdot\mathrm{s}^{-1}$
Air Probe	AoA α	$2.5\,\mathrm{deg}$
Air Probe	Side-slip angle β	$5\,\mathrm{deg}$
Surface encoders	Deflections u_a, u_e, u_r	$0.1\,\mathrm{deg}$

sensors used in this paper is provided in Table II, with the corresponding standard deviations σ. The sensors accuracy can vary by orders of magnitude, depending on the quality of the equipment chosen. In this paper, the standard deviations were chosen to reasonably match values commonly observed in the industry.

For the sake of simplicity, it is assumed in this paper that all sensors are sampled at the same frequency Δt_E, and that the sensors have no dynamics. At any time k, the measurement vector has dimension $\bar{Y}_k \in \mathbb{R}^{22}$. The weights Q_E in the MHE formulation (11) were chosen diagonal, with their entries taken as the inverse of the covariance of the noise of the corresponding sensor, i.e. $\{Q_E\}_i = \sigma_i^{-2}$. Similarly, the weight R_E was chosen as the inverse of the selected input noise $\sigma_{\dot{\mathcal{U}}} = 0.1\,\mathrm{deg}\cdot\mathrm{s}^{-1}$ introduced in the system, i.e. $R_E = \mathrm{diag}(0.1^{-2})$. The turbulence weights T_T and T_R were chosen in a similar way, using the covariance of Γ, Ω, $\dot{\Gamma}$ and $\dot{\Omega}$, extracted form the wind data.

C. NMPC formulation

The control formulation reads:

$$\begin{aligned} \min_{\mathcal{X},\mathcal{U}} \; & \sum_{k=i}^{i+N_\mathrm{P}} \|\bar{\mathcal{X}}_k - \mathcal{X}_k\|_Q^2 + \|\bar{\mathcal{U}}_k - \mathcal{U}_k\|_R^2 \qquad (12) \\ \text{s.t.} \quad & (1),(3),(6)-(10) \\ & \mathcal{X}_i = \hat{\mathcal{X}}_i,\ \Gamma_k = \hat{\Gamma}_i,\ \Omega_k = \hat{\Omega}_i \end{aligned}$$

Observe that the latest estimation of the translational and rotational turbulences $\hat{\Gamma}_i$ and $\hat{\Omega}_i$ are used in the NMPC scheme, and assumed constant over the prediction horizon $[t_i, t_{i+N_\mathrm{P}}]$. This is clearly a strong assumption, and devising a more reasonable integration of the estimated turbulences in the NMPC scheme is the object of current research.

The following constraints have been imposed on the system:

$$\begin{aligned} -5 \le \dot{r} \le 5, \quad -2 \le \ddot{r} \le 2 \\ -20 \le u_a \le 20, \quad -12.5 \le u_a \le 12.5, \\ -20 \le u_r \le 20, \quad -2.25 \le \dot{u}_r \le 2.25 \\ -20 \le u_e \le 20, \quad -3.25 \le \dot{u}_e \le 3.25 \end{aligned}$$

Note that the input bounds have been artificially tightened to demonstrate the capability of the proposed scheme to handle limited actuator capabilities. In practice, such bounds are typically relaxed, allowing the control scheme 12 to take stronger control actions, while the constraints are less often activated. The reference trajectory $\bar{\mathcal{X}}$, $\bar{\mathcal{U}}$ has been computed based on optimal control, the details are presented in [10].

D. Real-time iteration

After each iteration, the initial guess for problems (11)-(12) is updated by discarding the first element, shifting the state and input vectors X, U, and adding a new element at the end of the prediction horizon. The control inputs are updated by duplicating the last element,

and the states are updated using a forward integration on the last time interval.

If an initial value embedding is introduced in the subsequent problems [6], the first Newton step resulting from such an initial guess provides already a good approximation of the exact solution to problems (11)-(12), hence a real-time iteration (RTI) approach is used, where only one step per control interval needs to be performed. Moreover, most computations required to perform the first Newton step can be performed before the new initial conditions $\hat{\mathcal{X}}(t)$ are known. As a result, the re-calculation of the control inputs can be prepared before the new state estimation is known, and finished in a very short time once it becomes available, hence reducing significantly the delay between state estimation and control in the NMPC scheme [5].

E. Software approach

In this paper, numerical solutions to problem (11)-(12) were computed using the software ACADO Toolkit [15], based on direct multiple-shooting and RTI. The underlying parametric Quadratic Programs (QPs) are condensed and solved using a dense online primal active set strategy implemented in the software qpOASES [7].

SQP methods are known to be highly competitive in terms of computational speed for small to medium-scale parametric Nonlinear Programming (NLP) problems. However, the performance of alternative approaches such as interior-point techniques should be compared to the proposed approach. This comparison is beyond the scope of this paper.

The algorithms are implemented in code generation, where the compiled code is automatically tailored to the problem considered, and contains only the absolutely essential algorithmic components. Based on a symbolic representation of the optimal control problem to be solved online, problem-specific structure such as dimensions, sparsity patterns etc. is exploited during the code generation process to avoid irrelevant and redundant computations (see [16], [8])

IV. SIMULATION RESULTS

This section presents the results obtained using the model developed in Section II and the control scheme presented in Section III. The MHE and NMPC schemes were setup using the parameters displayed in table III. Fig. 1 displays the *xyz* trajectories of the wing. It can be observed that the control scheme exploits the cable length to cope with the

TABLE III
CONTROL PARAMETERS

Parameter	Value
NMPC horizon	10.82 [s]
MHE horizon	4.33 [s]
Sampling time	0.27 [s]
$x, y, z, r, \dot{r}$	10^{-4}
$\dot{x}, \dot{y}, \dot{z}$	10^{-3}
e_{ij}, ω_i	10^{-1}
$u_\mathrm{a}, u_\mathrm{e}, u_\mathrm{r}, \dot{u}_\mathrm{a}, \dot{u}_\mathrm{e}, \dot{u}_\mathrm{r}$	10^{0}

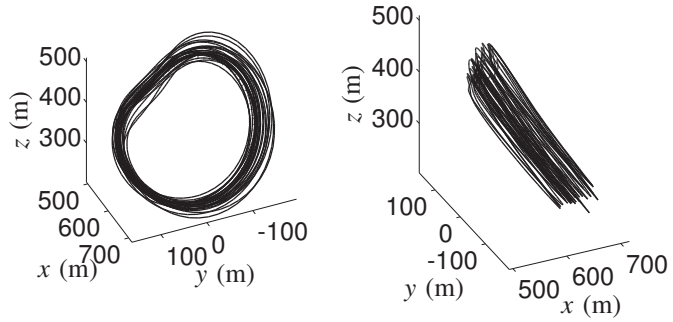

Fig. 1. System trajectories.

turbulences. A better tracking performance can be obtained by relaxing the input weights, resulting, however, in a loss of generated power. Fig. 3 displays the corresponding inputs. Fig. 4 displays the energy for the reference trajectory and the energy obtained from the system subject to turbulences. It can be seen that the system extracts more power than the reference trajectory, hence using the extra power available due to the turbulences. Fig. 5 displays the turbulences estimated by the MHE. The translational turbulences are well estimated, while the rotational turbulences are not accurately captured. The lack of accuracy in capturing the rotational turbulences is clearly the result of their limited observability. This difficulty is not a feature of the proposed MHE scheme but of the system itself, this observation will require further investigations to fully understand it. However, it was observed in simulations that, even though an estimation of the translational turbulences is crucial for obtaining good control performances, the poor estimation the rotational turbulences does not impact significantly the behaviour of the control scheme, and can actually be dismissed altogether. Further investigations are needed to fully understand these observations.

Fig. 6 displays the coefficient C_L and side-slip angle β. Both variables remain within the domain of validity of the aerodynamic model, moreover, the tether remains constantly under tension. Fig. 7 displays the time needed by the MHE and NMPC to compute updates of the estimation and control policy. The simulations were run on a single CPU clocked at 2.66 GHz. It can be observed that the time needed to perform the estimation update and control policy update are always lower that the sampling time, with a reasonable safety margin.

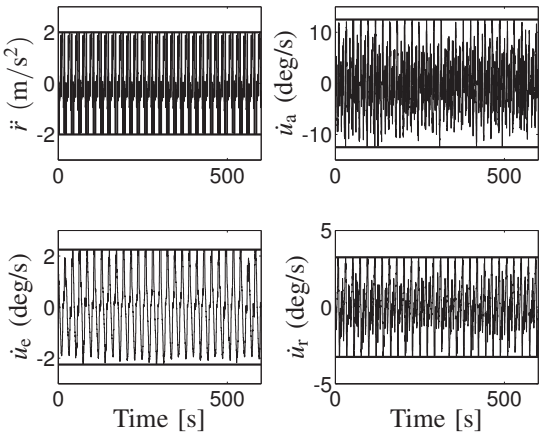

Fig. 2. Tether reeling acceleration and deflexion rate of the control surfaces

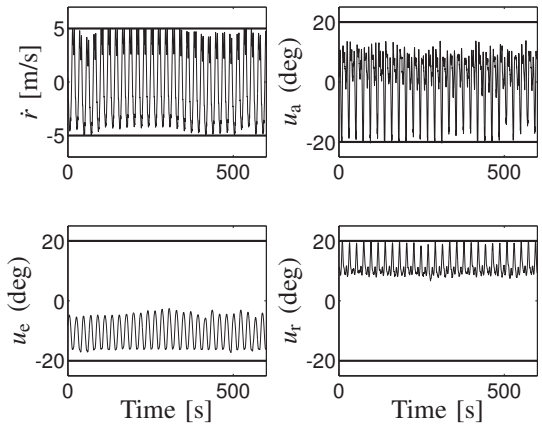

Fig. 3. Tether reeling speed and deflexion of the control surfaces

V. CONCLUSION & FUTURE WORK

This paper has presented a control scheme for an Airborne Energy System in power generation using pumping mode. The control scheme is based on Nonlinear Model Predictive Control (NMPC), combined with a Moving Horizon Estimation (MHE) observer. The proposed control technique was tested in simulations in a turbulent wind field. It performs the state estimation based on the fusion of a large number of sensors, and tracks the reference trajectories while handling the constraints of the system. The MHE provides an estimation of the wind turbulences. The control scheme was implemented in Code-Generation, resulting in a control scheme that is fast enough for a real-time implementation.

Future work will consider an MHE scheme with multiple sampling frequencies so as to better exploit the measurements provided by fast sensors. Using the simulation setup proposed here, the relevance of each sensor for the state and wind estimation will be studied. The penalty function in the NMPC scheme was arbitrarily chosen to yield a reasonably good trade-off between the tracking performance and the generated power. Future work will consider developing a penalty function that formally takes into account the performance in terms of generated power.

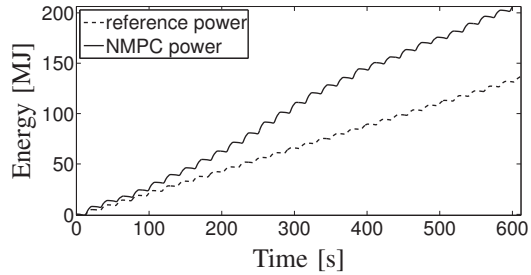

Fig. 4. Generated power, reference (dotted line), actual (plain line). The extra energy is yielded by the turbulences.

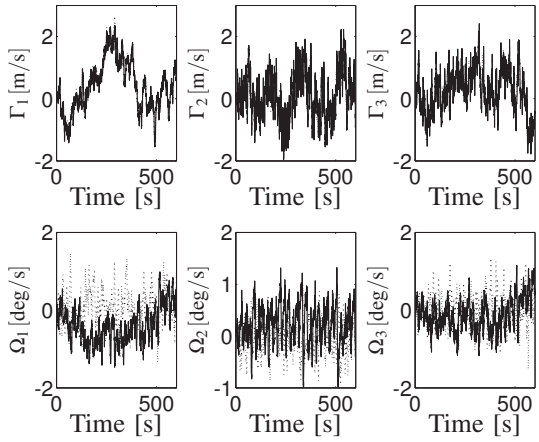

Fig. 5. Von Karman wind turbulences (dotted line) and the MHE wind estimation (plain line)

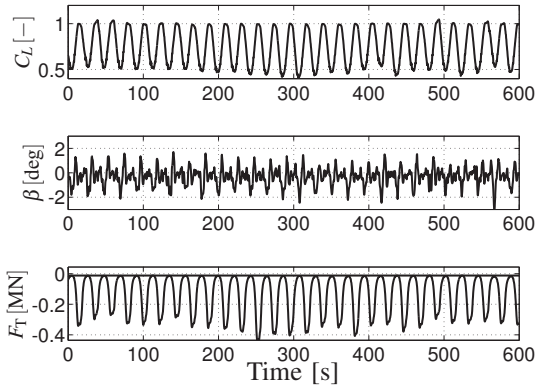

Fig. 6. Lift coefficient C_L, side-slip angle β, and thither force F_T.

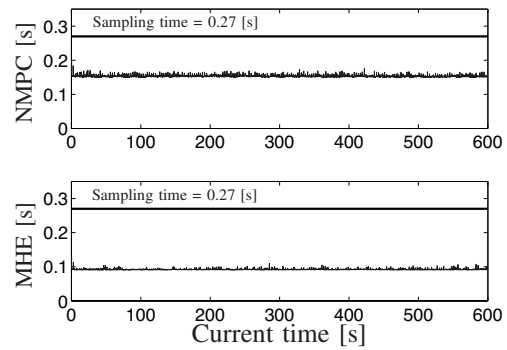

Fig. 7. Computational time per iteration for NMPC & MHE

VI. ACKNOWLEDGMENTS

This research was supported by Research Council KUL: PFV/10/002 Optimization in Engineering Center OPTEC, GOA/10/09 MaNet and GOA/10/11 Global real-time optimal control of autonomous robots and mechatronic systems. Flemish Government: IOF/KP/SCORES4CHEM, FWO: PhD/postdoc grants and projects: G.0320.08 (convex MPC), G.0377.09 (Mechatronics MPC); IWT: PhD Grants, projects: SBO LeCoPro; Belgian Federal Science Policy Office: IUAP P7 (DYSCO, Dynamical systems, control and optimization, 2012-2017); EU: FP7-EMBOCON (ICT-248940), FP7-SADCO (MC ITN-264735), ERC ST HIGHWIND (259 166), Eurostars SMART, ACCM.

REFERENCES

[1] L.T. Biegler. An overview of simultaneous strategies for dynamic optimization. *Chemical Engineering and Processing*, 46:1043–1053, 2007.

[2] H.G. Bock and K.J. Plitt. A multiple shooting algorithm for direct solution of optimal control problems. In *Proceedings 9th IFAC World Congress Budapest*, pages 243–247. Pergamon Press, 1984.

[3] E. A. Bossanyi. Further Load Reductions with Individual Pitch Control. *Wind Energy*, 8:481–485, 2005.

[4] Michael V. Cook. *Flight Dynamics Principles*. Elsevier Science, 2007.

[5] M. Diehl, H.G. Bock, J.P. Schlöder, R. Findeisen, Z. Nagy, and F. Allgöwer. Real-time optimization and Nonlinear Model Predictive Control of Processes governed by differential-algebraic equations. *Journal of Process Control*, 12(4):577–585, 2002.

[6] M. Diehl, R. Findeisen, S. Schwarzkopf, I. Uslu, F. Allgöwer, H.G. Bock, E.D. Gilles, and J.P. Schlöder. An Efficient Algorithm for Nonlinear Model Predictive Control of Large-Scale Systems. Part I: Description of the Method. *Automatisierungstechnik*, 50(12):557–567, 2002.

[7] H.J. Ferreau. An Online Active Set Strategy for Fast Solution of Parametric Quadratic Programs with Applications to Predictive Engine Control. Master's thesis, University of Heidelberg, 2006.

[8] H.J. Ferreau. *Model Predictive Control Algorithms for Applications with Millisecond Timescales*. PhD thesis, K.U. Leuven, 2011.

[9] S. Gros and M. Diehl. Attitude estimation based on inertial and position measurements. In *Conference on Decision and Control*, 2012.

[10] S. Gros and M. Diehl. A Relaxation Strategy for the Optimization of Airborne Wind Energy Systems. In *European Control Conference*, 2013.

[11] S. Gros, R. Quirynen, and M. Diehl. Aircraft Control Based on Fast Nonlinear MPC & Multiple-shooting. In *Conference on Decision and Control*, 2012.

[12] S. Gros, M. Zanon, and M. Diehl. Orbit Control for a Power Generating Airfoil Based on Nonlinear MPC. In *American Control Conference*, 2012. (submitted).

[13] S. Gros, M. Zanon, M. Vukov, and M. Diehl. Nonlinear MPC and MHE for Mechanical Multi-Body Systems with Application to Fast Tethered Airplanes. In *Proceedings of the 4th IFAC Nonlinear Model Predictive Control Conference, Noordwijkerhout, The Netherlands*, 2012.

[14] B. Houska and M. Diehl. Optimal Control for Power Generating Kites. In *Proc. 9th European Control Conference*, pages 3560–3567, Kos, Greece,, 2007. (CD-ROM).

[15] B. Houska, H.J. Ferreau, and M. Diehl. ACADO Toolkit – An Open Source Framework for Automatic Control and Dynamic Optimization. *Optimal Control Applications and Methods*, 32(3):298–312, 2011.

[16] B. Houska, H.J. Ferreau, and M. Diehl. An Auto-Generated Real-Time Iteration Algorithm for Nonlinear MPC in the Microsecond Range. *Automatica*, 47(10):2279–2285, 2011.

[17] J.H. Laks, L.Y. Pao, and A.D. Wright. Control of Wind Turbines: Past, Present, and Future. In *American Control Conference*, pages 2096–2103, 2009.

[18] M.L. Loyd. Crosswind Kite Power. *Journal of Energy*, 4(3):106–111, July 1980.

[19] Manwell, J. F., McGowan, J. G. and Rogers, A. L. *Wind Energy Explained: Theory, Design and Application, Second Edition*. John Wiley & Sons, Ltd, Chichester, UK, 2009.

[20] Pamadi. *Performance, Stability, Dynamics, and Control of Airplanes*. American Institute of Aeronautics and Astronautics, Inc., 2003.